ACTA MECHANICA SINICA (English Series), Vol.19, No.1, January 2002 ISSN 0567-7718
The Chinese Society of Theoretical and Applied Mechanics
Chinese Journal of Mechanics Press, Beijing, China
Allerton Press, INC., New York, U.S.A.

SIZE EFFECT AND GEOMETRICAL EFFECT OF SOLIDS IN MICRO-INDENTATION TEST*

WEI Yueguang (魏悦广)† WANG Xuezheng (王学峥) ZHAO Manhong (赵满洪)
CHENG Che-Min (郑哲敏) BAI Yilong (白以龙)
(*LNM, Institute of Mechanics, Chinese Academy of Sciences, Beijing* 100080, *China*)

ABSTRACT: Micro-indentation tests at scales of the order of sub-micron show that the measured hardness increases strongly with decreasing indent depth or indent size, which is frequently referred to as the size effect. At the same time, at micron or sub-micron scale, another effect, which is referred to as the geometrical size effects such as crystal grain size effect, thin film thickness effect, etc., also influences the measured material hardness. However, the trends are at odds with the size-independence implied by the conventional elastic-plastic theory. In the present research, the strain gradient plasticity theory (Fleck and Hutchinson) is used to model the composition effects (size effect and geometrical effect) for polycrystal material and metal thin film/ceramic substrate systems when materials undergo micro-indenting. The phenomena of the "pile-up" and "sink-in" appeared in the indentation test for the polycrystal materials are also discussed. Meanwhile, the micro-indentation experiments for the polycrystal Al and for the Ti/Si_3N_4 thin film/substrate system are carried out. By comparing the theoretical predictions with experimental measurements, the values and the variation trends of the micro-scale parameter included in the strain gradient plasticity theory are predicted.

KEY WORDS: micro-indentation tests, size effect, geometrical effect, strain gradient plasticity

1 INTRODUCTION

Indentation test is an important and effective experimental method, and has been used extensively to estimate the plastic properties of solids undergoing plastic deformation. Through indentation test, the loading-unloading relation between hardness and indent depth is measured. Thereby, the material parameters, such as the yielding stress, strain hardening exponent, Young's modulus, etc. are estimated. Recently, with the advancement of experimental technique and measuring precision, it is possible to carry out the indentation tests at the scale of one micron or sub-micron for obtaining more detailed material information. Such small-scale indentation experiments are frequently referred to as micro-indentation tests (or nano-indentation tests). In the micro-indentation test, new results, different from the conventional ones, the size-dependent results, were obtained extensively[1~9]. For metal materials, the measured hardness may double or even triple the conventional hardness as the indent size (or depth) decreases to a fifth micron. The effect is often referred to as the size effect. In addition, at the micron scale, if material is of some micro-geometrical structures and if the geometrical structure size is comparable to the indent depth, the size-dependent hardness mentioned above may be influenced additionally by the geometrical size. We call this effect as the geometrical effect in the present research. However, the trends of both size effect and geometrical effect are at odds with the size-independence implied by the conventional elastic-plastic theory. Otherwise, from a dimensional consideration[10], the hardness was only dependent of macroscopic parameters of material, i.e., was size-independent.

In order to predict the size effect phenomena, recently, several strain gradient plasticity theories have been developed[11~13]. These theories include the strain gradient effects and go beyond the conventional elastic-plastic theory frame. In the new constitutive

Received 30 April 2001, revised 29 October 2001
* The project supported by the National Natural Science Foundation of China (19891180 and 19925211) and Bai Ren Plan of CAS
† E-mail: ywei@lnm.imech.ac.cn

relations, the strain terms are matched with the new strain gradient terms through several length parameters. Thus the material size effect can be characterized by the length-scale parameters.

On the researches of the size effect in the indentation tests by using strain gradient plasticity theories, in Ref.[4], the case when the micro-scale parameter was smaller than the contact radius was analyzed by adopting the couple stress theory[11] under an incompressible assumption. In Ref.[3], the similar case to [4] but adopting the Fleck and Hutchinson's strain gradient plasticity[11] was analyzed. By applying the prediction result to the micro-indentation test for material tungsten (W)[8], the micro-scale parameter for material W was obtained within 0.25∼0.52 μm.

Alternatively, a dislocation model has been used to study the size effect for the micro-indentation test in Ref.[1]. By using the Taylor's relation, von Mises' plastic flow law and the conventional relation of the hardness (triple the flow stress), an inverse square root relation between hardness and indent depth was obtained.

Comparing the micro-indentation test results for conventional metals (Cu, Ag, Al)[2,7,9] with that for the uniquely high modulus metal W[8], it is clear that the sensitive zone scale of the size effect of the former is smaller than that of the latter for an order of magnitude. Correspondingly, the scale of the contact radius of the former is also smaller than that of the latter for an order of magnitude. Furthermore, in view of the previous investigations[3,4] which were focused on the case when the micro-scale parameter was smaller than the contact radius, it is necessary to discuss the case when the micro-scale parameter is greater, even several times greater than the contact radius for the conventional metals (Cu, Ag, Al, etc.). Following [9], in the present research, the Fleck and Hutchinson's strain gradient plasticity model[11], and a compressible general constitutive relation are considered. Experimental researches of the micro-indentation tests for polycrystal aluminum and the metal thin film/ceramic substrate system are carried out. For the polycrystal Al, the experimental programming adopted here is different from the conventional continuum stiffness method (CS method), and the measured hardness curve is based on a unique loading point on the surface, and depends on the status of the loading point. In the present experiment, many loading points are selected randomly, and one test point corresponds to only one measured value for hardness/depth relation. Although a data strip for hardness/depth relation will be obtained by using the CS method, its defects can be avoided. By comparing the theoretical prediction with the strip test data, the micro-scale parameter and its variation trends for different material can be predicted. For comparison, in the indentation experiment for the Ti/Si_3N_4, a thin film/substrate system, the CS method will be adopted. Through comparing the theoretical predictions with the experimental results, the values and the variation trends of the micro-scale length parameter for different material, related with micro-geometrical size, are predicted.

2 DEFORMATIONAL THEORY OF STRAIN GRADIENT PLASTICITY

In the present section, the compressible general form of the deformational theory of the strain gradient plasticity is outlined as follows.

2.1 Constitutive Relations

The definitions of the strain and strain gradient are

$$\begin{aligned} \varepsilon_{ij} &= \frac{1}{2}\left(u_{i,j}+u_{j,i}\right)=\varepsilon_{ij}^{\mathrm{e}}+\varepsilon_{ij}^{\mathrm{p}} \\ \eta_{ijk} &= u_{k,ij}=\eta_{ijk}^{\mathrm{e}}+\eta_{ijk}^{\mathrm{p}} \end{aligned} \tag{1}$$

The expressions related with the constitutive relations are listed as follows

$$\begin{aligned} W^{\mathrm{e}} &= E\left(\frac{\nu}{2(1+\nu)(1-2\nu)}\varepsilon_{kk}^{\mathrm{e}2}+\frac{1}{2(1+\nu)}\varepsilon_{ij}^{\mathrm{e}}\varepsilon_{ij}^{\mathrm{e}}+\right. \\ &\quad \left.\sum_{I=1}^{4}L_I^{\mathrm{e}2}\eta_{ijk}^{\mathrm{e}(I)}\eta_{ijk}^{\mathrm{e}(I)}\right) \\ \sigma_{ij} &= \partial W^{\mathrm{e}}/\partial\varepsilon_{ij}^{\mathrm{e}} \qquad \tau_{ijk}=\partial W^{\mathrm{e}}/\partial\eta_{ijk}^{\mathrm{e}} \\ \Xi &= \sqrt{\frac{2}{3}\varepsilon'_{ij}\varepsilon'_{ij}+\sum_{I=1}^{3}L_I^2\eta_{ijk}^{(I)}\eta_{ijk}^{(I)}} \\ \Sigma &= \sqrt{3J_2}=\sqrt{\frac{3}{2}\sigma'_{ij}\sigma'_{ij}+\sum_{I=1}^{3}L_I^{-2}\tau_{ijk}^{(I)}\tau_{ijk}^{(I)}} \\ \eta_{ijk}^{(I)} &= T_{ijklmn}^{(I)}\eta_{lmn} \qquad \tau_{ijk}^{(I)}=T_{ijklmn}^{(I)}\tau_{lmn} \\ \varepsilon_{ij}^{\mathrm{p}} &= \frac{3}{2h^{\mathrm{p}}}\frac{\partial J_2}{\partial\sigma_{ij}}=\frac{3}{2h^{\mathrm{p}}}\sigma'_{ij} \\ \eta_{ijk}^{\mathrm{p}} &= \frac{3}{2h^{\mathrm{p}}}\frac{\partial J_2}{\partial\tau_{ijk}}=\frac{1}{h^{\mathrm{p}}}\sum_{I=1}^{3}L_I^{-2}T_{ijklmn}^{(I)}\tau_{lmn} \\ h^{\mathrm{p}} &= \Sigma/(\Xi-\Sigma/E) \end{aligned} \tag{2}$$

where Σ and Ξ are the effective stress and effective

strain, respectively. L_I^{e} and $L_I (I = 1, 4)$ are the micro-scale parameters for the elastic and plastic case, respectively. From the discussion in [11], there exists a general relation among the micro-scales (SG theory)

$$L_1 = L \qquad L_2 = \frac{1}{2}L \qquad L_3 = \sqrt{\frac{5}{24}}L \tag{3}$$

In addition, take $L_4 = L/2$. Similarly, (3) is valid also for the elasticity strain gradient case, with L replaced by L^{e} in (3). Moreover, the previous research has shown that the solution is insensitive to the value of L^{e}/L within the region $0 < L^{\mathrm{e}}/L < 1$[14]. Thus, take $L^{\mathrm{e}}/L = 0.5$ in the present research. In the last relation of (2), h^{p} is the effective plastic modulus. Considering the strain hardening material

$$\begin{aligned} \Xi &= \Xi_0 \left(\Sigma/\sigma_Y\right) && \Sigma \le \sigma_Y \\ \Xi &= \Xi_0 \left(\Sigma/\sigma_Y\right)^{1/N} && \Sigma > \sigma_Y \end{aligned} \tag{4}$$

we have

$$h^{\mathrm{p}} = E\Big[\left(\Sigma/\sigma_Y\right)^{1/N-1} - 1\Big]^{-1} \tag{5}$$

In formula (2), $T^{(I)}_{ijklmn} (I = 1, 4)$ is the projection tensor of the strain gradient, and the detailed expressions are given in [14]. Thus, by using the formulas (1) and (2) and the projection tensor normality, the compressible general form of the deformational theory of the strain gradient plasticity can be expressed as

$$\begin{aligned} \sigma_{ij} = {} & \frac{E}{1+\nu+\dfrac{3}{2}E/h^{\mathrm{p}}}\varepsilon_{ij} + \\ & \frac{1}{3}\left(\frac{E}{1-2\nu} - \frac{E}{1+\nu+\dfrac{3}{2}E/h^{\mathrm{p}}}\right)\varepsilon_{kk}\delta_{ij} \\ \tau_{ijk} = {} & 2E\left(\sum_{I=1}^{3}\frac{L_I^2}{L_I^2/L_I^{\mathrm{e}2}+2E/h^{\mathrm{p}}}T^{(I)}_{ijklmn} + \right. \\ & \left. L_4^{\mathrm{e}2}T^{(4)}_{ijklmn}\right)\eta_{lmn} \end{aligned} \tag{6}$$

2.2 Equilibrium and Variational Relations

Frequently, equilibrium equations can be described by the displacement-variational relation, for the finite element implementation. The displacement-variational relation for the strain gradient plasticity theory is given by[11]

$$\begin{aligned} \int_V \left(\sigma_{ij}\delta\varepsilon_{ij} + \tau_{ijk}\delta\eta_{ijk}\right)\mathrm{d}V = {} & \int_V f_k\delta u_k \mathrm{d}V + \\ & \int_S t_k\delta u_k \mathrm{d}S + \int_S r_k\left(\mathrm{D}\delta u_k\right)\mathrm{d}S \end{aligned} \tag{7}$$

Based on (7), the traction on S is defined by

$$\begin{aligned} t_k = {} & n_i\left(\sigma_{ik} - \frac{\partial\tau_{ijk}}{\partial x_j}\right) + n_i n_j \tau_{ijk}\left(\mathrm{D}_p n_p\right) - \\ & \mathrm{D}_j\left(n_i\tau_{ijk}\right) \end{aligned} \tag{8}$$

and the surface torque by $r_k = n_i n_j \tau_{ijk}$. The operators D and D_j in (7) and (8) are defined as

$$\mathrm{D}_j = \partial/\partial x_j - n_j n_k \partial/\partial x_k \qquad \mathrm{D} = n_k \partial/x_k \tag{9}$$

where n_i in (7)$\sim$(9) is the direction cosine on S.

3 PROBLEM FORMULATIONS

3.1 Boundary Conditions of Indentation Test Problem

Consider that the pressure head is a circular cone. The usual pyramid pressure head can be replaced approximately with a circular cone according to the cross-section area equivalence for simplifying the analysis. A traction condition on the remote boundary is used here, instead of the displacement boundary conditions as is usually done. The advantages of such a treatment are in either catching the fundamental feature of indentation test, or making the description and analysis much simpler.

Elastic stress distributions on the remote boundary are given by (see Fig.1)[15]

$$\begin{aligned} \sigma_r &= \frac{P}{2\pi\bar{r}^2}\left(\frac{1-2\nu}{1+\sin\theta} - 3\cos^2\theta\sin\theta\right) \\ \sigma_z &= -\frac{3P}{2\pi\bar{r}^2}\sin^3\theta \\ \sigma_{rz} &= -\frac{3P}{2\pi\bar{r}^2}\cos\theta\sin^2\theta \\ \sigma_\varphi &= \frac{(1-2\nu)P}{2\pi\bar{r}^2}\left(\sin\theta - \frac{1}{1+\sin\theta}\right) \end{aligned} \tag{10}$$

where $\bar{r}^2 = r^2 + z^2$. The definitions of the others are shown in Fig.1. The mixed boundary conditions on the material surface ($z = 0$) for the small deformation case are

$$\begin{aligned} & u_z = -r\tan\beta && R_r = 0 \\ & R_z \le 0 && 0 \le r \le R = h/\tan\beta \\ & R_r = R_z = 0 && R \le r \end{aligned} \tag{11}$$

where the reference (original) point of vertical displacement u_z is chosen at the conical apex, R is the contact radius, h is the penetration depth of the indenter, R_r and R_z are the surface tractions.

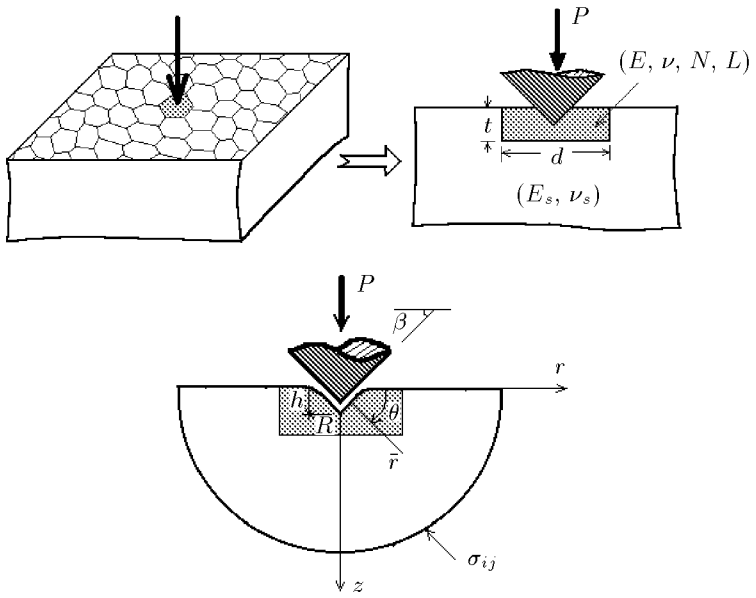

Fig.1 Simplified model for polycrystal material undergoing the micro-indent

For the convenience of the analysis, define a loading-length parameter as

$$R_0 = \sqrt{P/(3\pi\sigma_Y)} \tag{12}$$

R_0 is the conventional contact radius (when the size effect is neglected) for the low-hardening metal material in the case of flat pressure head[16]. The hardness definition and the relations with the geometrical parameter and indent depth are

$$H = \frac{P}{\pi R^2} = 3\sigma_Y \left(\frac{R_0}{R}\right)^2 = 3\sigma_Y \left(\frac{R_0}{h}\tan\beta\right)^2 \tag{13}$$

3.2 Polycrystal Material Undergoing the Micro-Indent

Consider a polycrystal material whose crystal grain size is comparable with the indent depth. In this case, the geometrical effect on the hardness must be considered. When the pressure head is applied to a crystal grain on the material surface, the plastic slip zone will be constrained to the region of the crystal grain until the pressure head approaches the grain boundary, due to the shielding effect of the grain boundary. Effects of all other crystal grains can be approximately described by an elastically and homogeneously equivalent body with Young's modulus and Poisson's ratio (E_s, ν_s) by using the Hill's consistent approach[17]. The equivalent Young's modulus value E_s for the polycrystal material is smaller than E, the equivalent Young's modulus of the single crystal material. The simplified model for polycrystal material undergoing a micro-indent is shown in Fig.1. t is the crystal grain size in the indent direction, d is another size of the crystal grain.

In all relations given above, all parameters or variables with length dimension can be normalized by R_0, and all quantities with stress dimension can be normalized by σ_Y, such that the normalized hardness can be taken to be a function of the independent and non-dimensional parameters as follows

$$\frac{H}{\sigma_Y} = f\left(\frac{E}{\sigma_Y}, \frac{E_s}{E}, \nu, \nu_s, N, \beta, \frac{L}{R_0}, \frac{t}{R_0}, \frac{t}{d}\right) \tag{14}$$

while contact radius and indent depth are related to the hardness by (13). The detailed expression of (14) will be implemented by solving the indentation problem numerically, using the strain gradient plasticity theory.

3.3 Thin Film/Substrate System Undergoing the Micro-Indent

Additionally, consider a metal thin film/ceramic substrate system undergoing the micro-indent on the surface of a thin film. When the thickness of the thin film is comparable with the indent depth, the effect of the geometrical size on the hardness must be considered. In this case, the hardness-parameter relation can be written as

$$\frac{H}{\sigma_Y} = f\left(\frac{E}{\sigma_Y}, \frac{E_s}{E}, \nu, \nu_s, N, \beta, \frac{L}{R_0}, \frac{t}{R_0}\right) \tag{15}$$

where t is the thin film thickness, E_s is Young's modulus of the substrate material. For metal thin film/ceramic substrate system, usually, $E_s/E \approx 6$. Simplified model for thin film/substrate system undergoing the micro-indent is shown in Fig.2.

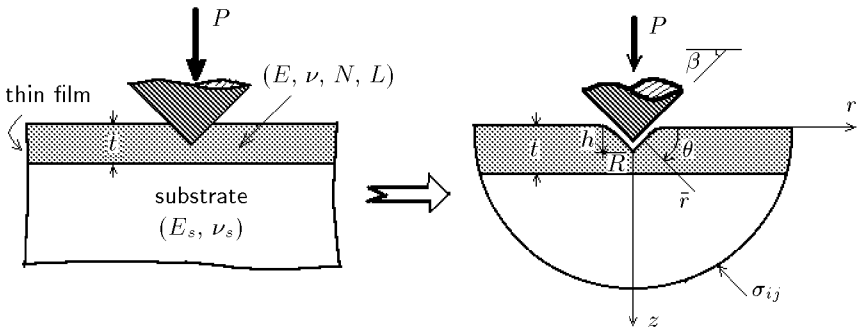

Fig.2 Simplified model for the metal thin film/ceramic substrate system undergoing the micro-indent

4 FINITE ELEMENT METHOD FOR THE DEFORMATIONAL THEORY OF THE STRAIN GRADIENT PLASTICITY

For the constitutive relation that takes account of the strain gradient effect, generally speaking, the conventional finite element method can not be used, and a special finite element method with the displacement derivatives as the nodal variables is needed[13,18,19]. However, for the stretching-dominated strain gradient plasticity problem, one can obtain an effective result by adopting the iso-parametric displacement element with nine nodes[14,19,20]. Obviously, the indentation problem is stretching-dominated. Therefore, in the present analysis, such an element will be used. In addition, 2×2 Gauss integration points are adopted for each element.

For the axisymmetrical problem of indentation test, consider that the elastic stress field acts on the remote boundary, and the pressure head apex is taken as the reference point (zero point) of vertical displacement. Thus, imagine that under the action of the remote stress field, material would move back to the pressure head surface, near the apex, material would contact with conical surface, and the contact radius would be equal to R. The displacement constraint conditions in the contact region are described by (11).

Using the plastic deformational theory, the solution procedures can be outlined as follows. Firstly, calculate the elastic solution. Secondly, taking elastic solution as the initial trial, find the solution for the higher-hardening material by iterating. Thirdly, taking the last solution as the new initial trial, find the convergent solution for the lower-hardening material case by iterating. For example, the solution procedures for $N = 0.1$ case are described as follows. Firstly, finding the elastic solution and then taking it as the initial solution, calculate the convergent solution for $N = 0.3$ case by iterating. Secondly, taking the last solution ($N = 0.3$) as a new initial trial, find the convergent solution for the case of $N = 0.2$ by iterating. Finally, based on the solution of $N = 0.2$, find the convergent solution for $N = 0.1$ by iterating.

For the true case of the micro-indentation test problem, take the remote boundary as the reference point of vertical displacement. Thus, the vertical displacement field can be expressed by

$$v(r, z) = u_z(r, z) - u_z^{\infty} \tag{16}$$

where u_z^{∞} is the vertical displacement at the remote boundary for case when the conical apex is defined as the reference point of vertical displacement. The form of finite element mesh adopted in the present research is simply fan-shaped using the axisymmetrical condition.

5 NUMERICAL AND EXPERIMENTAL RESULTS FOR POLYCRYSTAL MATERIAL

5.1 Numerical Results

In the numerical analyses for the conventional metal materials, material parameters are taken as $(E/\sigma_Y, \nu, N) = (300, 0.3, 0.1)$ and the flat pressure head case ($\beta = 20°$) is considered. Firstly, the relations of the hardness against the normalized length parameter and the normalized crystal grain size are predicted (see (14)). Secondly, the relations of the hardness against the indent depth and crystal grain size are obtained. The size effect and geometrical effect in the micro-indentation test can be obviously identified. Note that the conventional flat pyramid cone pressure head will be equivalently replaced by the flat circular conical head for the convenience of analysis, and the equivalent conical angle β is about 20 degrees. Therefore, in the present research, the pressure head angle is taken as $\beta = 20°$.

Figure 3 shows the relation between the normalized hardness and the normalized material length parameters and the normalized crystal grain sizes. The normalizing quantity of hardness ($3\sigma_Y$) is the hardness value for the typical metal materials when the size effect is neglected. The normalizing quantity (R_0) for the length parameter and for the crystal grain size is the load-length parameter, which is the radius of the contact zone when the size effect is not considered. In Fig.3, a wide region of the normalized quantity L/R_0 from 0 to 3 and a wide region of t/R_0 are considered. From Fig.3, the hardness increases with L/R_0 quickly, especially for small value of t/R_0. As t/R_0 increases from 0.364 ($\tan 20°$) to 10, the hardness curve decreases very quickly at starting, and then approaches a stable value, which corresponds to a homogeneous material hardness curve (where the geometrical effect is very weak). Note that the material hardness sharply increases when the indent depth approaches the crystal grain size value ($h = 0.364R$).

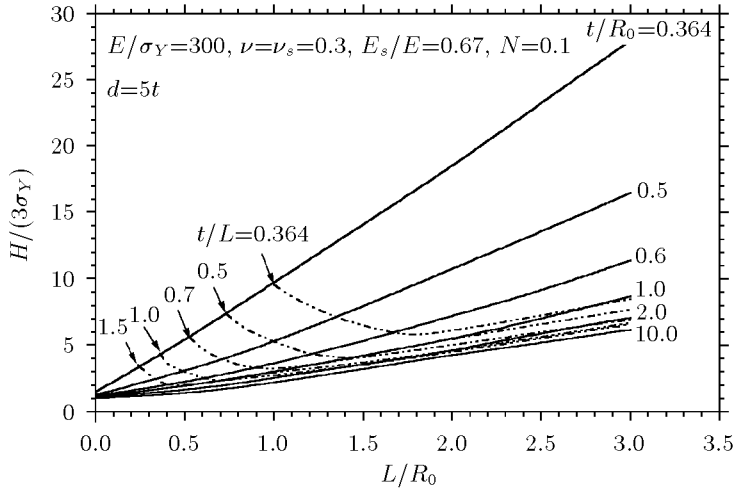

Fig.3 Variation of hardness with normalized parameters: length parameter L/R_0, grain size t/R_0, and t/L

Figure 3 shows the case when the crystal grain size is larger than $0.364R_0$ (the indent depth for conventional material). The effect of the normalized parameter t/R_0 on the hardness characterizes either the crystal grain size effect, or the load effect. When the composition parameter value is small, it is either a small crystal grain size case when applied load is fixed or a big load case when grain size is fixed. In order to explain the effect of the crystal grain size, isolines of the normalized parameter t/L are plotted based on the hardness relation against L/R_0 and t/R_0, see dashed lines shown in Fig.3. We also investigate the influence of Young's modulus E_s of the equivalent body on the material hardness. The results are shown in Fig.4. From Fig.4, clearly, the influence of the Young's modulus Ratio E_s/E on the material hardness is very weak within a wide region of $E_s/E = 0.67$ to 6.70.

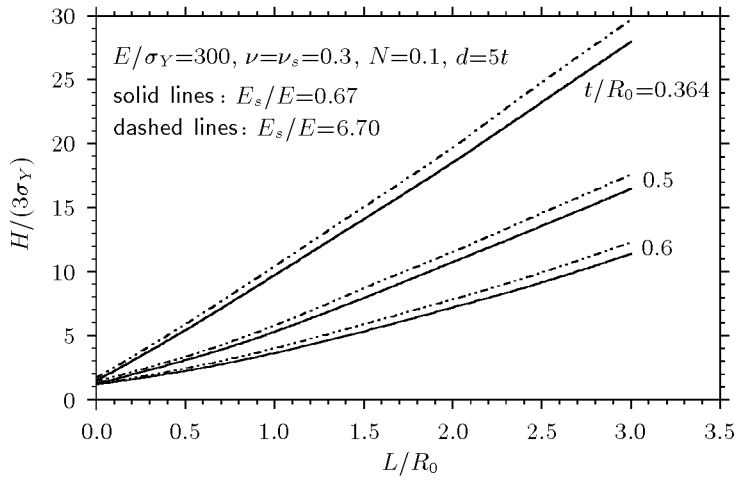

Fig.4 The influence of Young's modulus ratio on the hardness curves

Furthermore, the dashed lines in Fig.3 can be replotted in the coordinates: hardness/indent depth, see Fig.5. From Fig.5, the size effect and the crystal grain size effect are clearly shown. When the indent depth is small, i.e., when the indent tip is far away from the crystal boundary, the size effect is dominant. As the indent depth increases, the size effect decreases and the geometrical effect increases. When the indent depth approaches the grain boundary, the geometrical effect becomes dominant and makes the hardness curve sharply go up. With the decrease of the crystal grain size, both the size effect and crystal geometrical size effect are enlarged. The effects of the crystal grain size d and the size in the horizontal direction on the material hardness are shown in Fig.6. In Fig.6, the geometrical effects for two values of d, $d = 5t$ and $d = 100t$, respectively, are displayed. The results show that the effect of the crystal grain size in the horizontal direction on the material hardness is very weak. The conclusion implies that although the analysis is for the polycrystal material, it can approximately be applied for the thin film/substrate system to be discussed in the next sub-section.

The phenomena of "pile-up" and "sink-in" in the micro-indentation test for the polycrystal material are also investigated here. The results are shown in Fig.7. From Fig.7, with the increase of the material length parameter or with the decrease of the applied load ($R_0 = \sqrt{P/3\pi\sigma_Y}$), correspondingly with the increase of L/R_0, the "pile-up" phenomenon disappears and the "sink-in" feature gets prominent in the micro-indentation test. The pile-up phenomenon is favorable for the big force and small length parameter. This conclusion is consistent with the single crystal material case[9]. When the crystal grain size is large, the geometrical effect is weak, and the size effect is dominant. As the crystal grain size decreases, the geometrical effect increases, and the indent depth decreases considerably for a fixed applied load.

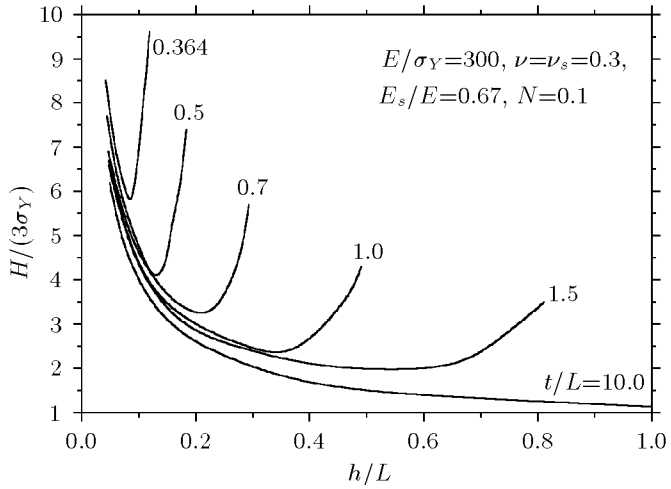

Fig.5 Size effect and geometrical effect on the hardness/depth relations

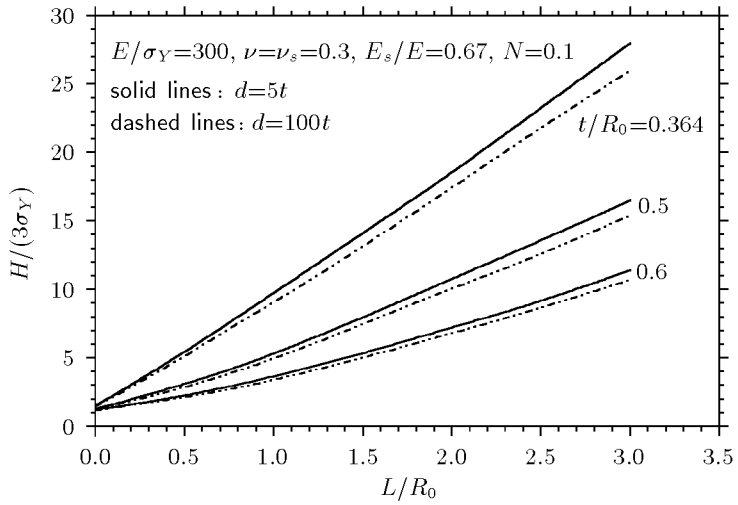

Fig.6 Effect of the crystal grain size in the horizontal direction on the hardness

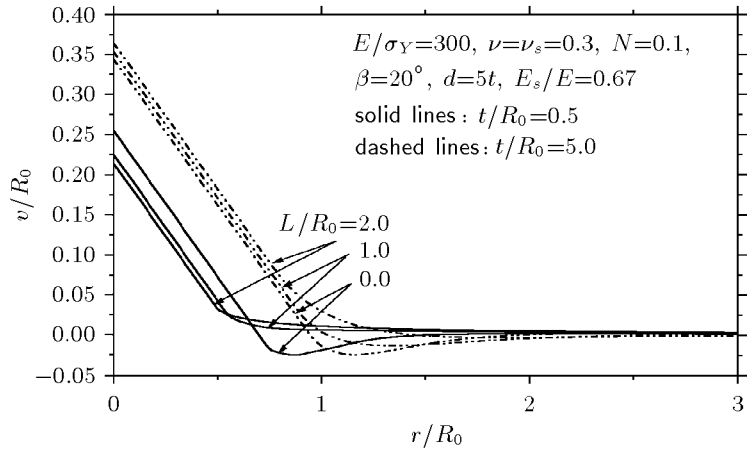

Fig.7 The simulation of the phenomena "pile-up" and "sink-in" for polycrystal in micro-indentation test

5.2 Micro-Indentation Experiment for Polycrystal Al

In order to study the micro-geometrical effects experimentally, we design the test specimens for polycrystal Al with several different crystal grain sizes. The indentation experimental method is similar with Ref.[9] for the single crystal material. The experimental method consists of choosing many loading points arbitrarily on the specimen surface, and for one loading point, only one set of experimental data about hardness and indent depth being obtained. In such a method we shall obtain a data strip about the hardness/indent depth relation. The scatter degree of the data strip depends on the feature of the selected loading point on the specimen surface. If an indent point is just located at a fault region on the specimen surface, a low hardness will be obtained, when the indent depth is fixed. If an indent point is just chosen at a hard particle, a high hardness value is obtained. Figure 8 shows the surface profile of the polycrystal Al specimen for a SE photograph. From Fig.8, on the specimen surface, some faults exist inevitably. If the continuum stiffness method is used, the obtained hardness curve must depend on the indent location. Therefore, we shall use the experimental method here by selecting the indent loading points on the specimen surface arbitrarily as in [9], rather than adopting the continuum stiffness method, so that the influence of the faults and the different loading point selections on the experimental results will be displayed clearly.

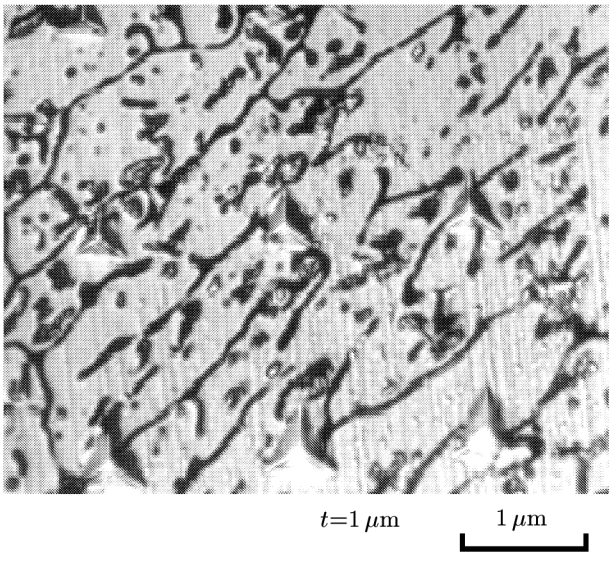

Fig.8 The profile of the specimen surface for the polycrystal Al

In Fig.9, the experimental hardness results for polycrystal Al for several crystal grain sizes are shown. From Figs.9(a) to (d), the series of the grain sizes, 0.6 μm, 1 μm, 2 μm and infinitly large size (single crystal Al), are shown separately. The results show that the feature of the hardness variation with the indent depth is in a "U" form. When the indent depth is small, a strong size effect is characterized. As the indent depth increases, the hardness decreases and passes through a lower limit value, then increases with the indent tip approaching the grain boundary. Comparing the results shown in Figs.9(a), (b), (c) and (d) for different crystal grain sizes, with the decrease of the crystal grain size, the hardness increases in general. For comparison, the theoretical predictions of the hardness using the strain gradient plasticity are also shown in Fig.9. For each case, two curves corresponding to different length parameter values are plotted. These two curves can be taken as the bounds of the experimental data. As the crystal grain size increases, the length parameter values decrease, and approach 1 μm and 2 μm, corresponding to the lower bound curve and upper bound curve, respectively, for the single crystal case. The material hardness approaches the conventional value as the indent depth increases infinitely. For the single crystal case, the curve feature of the hardness variation with the indent depth is in an "L" form.

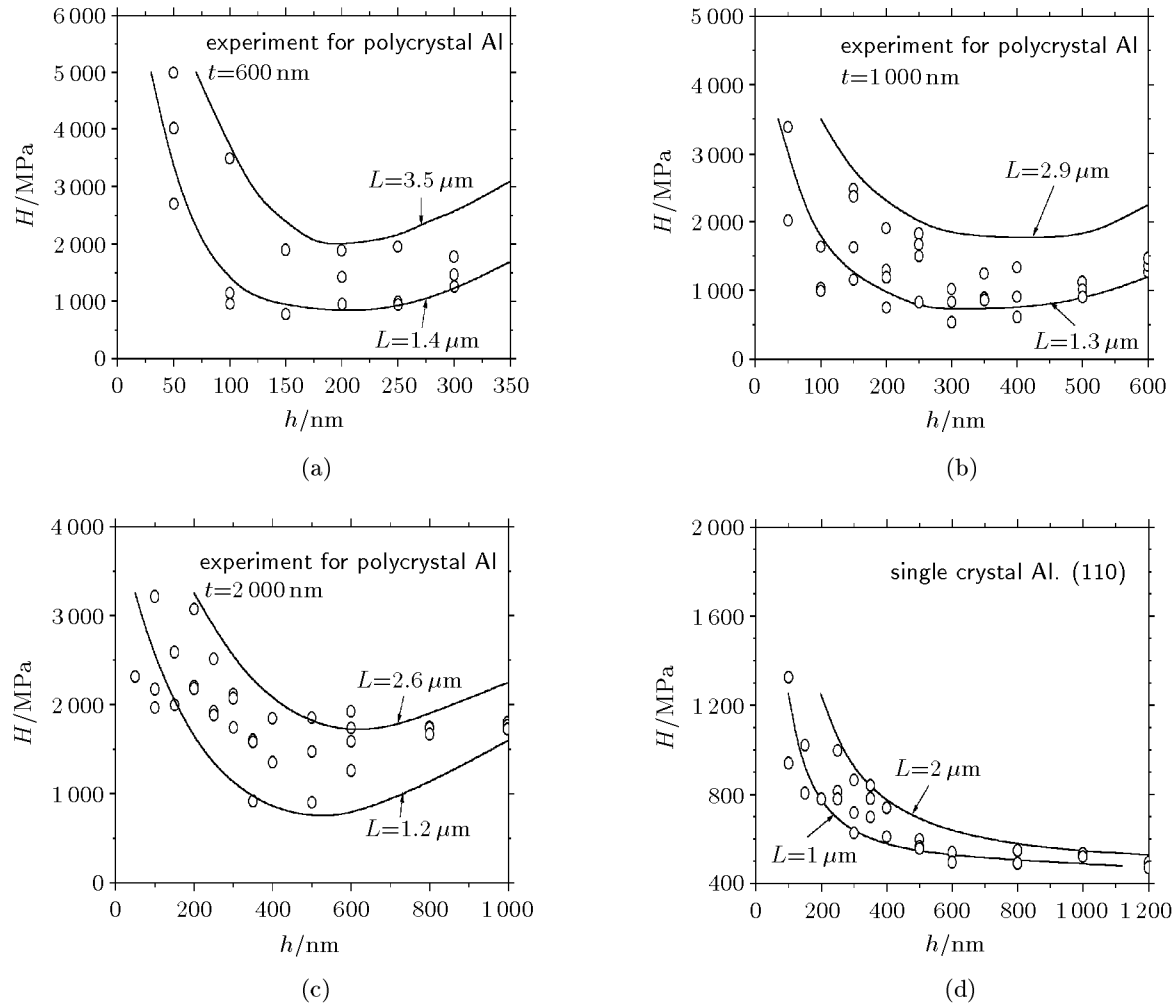

Fig.9 Experimental and numerical results of the hardness/indent depth relations for different crystal grain sizes

As mentioned above, if one adopts the method of arbitrarily selecting the loading points on the specimen surface in the indentation experiment, one will obtain the hardness variations with the indent depth in the form of the data strip. Figure 9 shows such strips, the scattered data strips. Obviously, the width of the scattered strip of the hardness for the polycrystal specimen is somewhat larger than that for the single-crystal specimen, comparing Figs.9(a), (b), (c) with Fig.9(d). This result is reasonable and seems to

be expected. This is because for a polycrystal specimen the experimental hardness is influenced both by the loading point status (faults, reinforced-particles, etc.) as for a single-crystal specimen case, and by the grain boundaries and the grain size differences. The latter effect is specifically important for the present research case when indent depths are comparable with the grain sizes. Although the polycrystal specimen is expected consisting of the uniform grain size, it is rarely the case. From the SE photograph of the surface profile for a polycrystal Al specimen with $1\,\mu$m grain size shown in Fig.8, besides the many faults being observed on the surface, the grain sizes are not uniform. In Fig.8, the longer black curves characterize the grain boundaries and the small black zones are the faults. Some indent loading locations are clearly observed in the figure.

6 Ti FILM LAIN ON THE Si_3N_4 CERAMIC SUBSTRATE UNDERGOING MICRO-INDENTING

Let us discuss the hardness of a thin film lain on a ceramic substrate. When the thin film thickness is comparable with the indent depth, the substrate and film/substrate interface will have a strong influence on the hardness (geometrical effect). In the present case, the parameter relation between hardness and other material and geometrical parameters is given in (15).

From discussions in subsection 4.1, the predicted hardness relation for the polycrystal material shown in Fig.5 can be applied to the thin film/substrate system approximately within a parameter region $0.67 < E_s/E < 6.70$. In the present case, the Young's modulus ratio for the ceramic substrate (Si_3N_4) and metal thin film (Ti) is about 6.0. In order to investigate the hardness variation with the thin film thickness, we have designed three kinds of the specimens corresponding to a series of the thin film thickness. For a comparison, we adopt the conventional continuum stiffness method in the experiment, i.e., the curve of the hardness variation with the indent depth is obtained from one loading point on the specimen surface. In such a test method, the experimental hardness curve will be a smooth one.

Figure 10 shows the experimental hardness for the Ti film lain on the Si_3N_4 substrate for three different thicknesses of the thin film. Figures 10(a), (b) and (c) correspond to the thin film thickness $1.2\,\mu$m, $1.8\,\mu$m and $13\,\mu$m, respectively. From Fig.10, the feature of the hardness variation with the indent depth is in a "U" form and it can be described as follows: When indent depth is small, the result shows a strong size effect. As the depth increases, the hardness decreases quickly until the indent depth reaches some fraction of the thin film thickness, the hardness assumes a lowest value. From the lowest value the hardness turns to increase as the indent depth increases further. Alternatively, as the thin film thickness increases, the hardness decreases all over the region and the depth value corresponding to the lowest hardness point increases. When the thin film thickness increases to a certain extent ($13\,\mu$m), the influence of thin film thickness on the hardness curve can be neglected, so that the hardness/depth curve approaches the conventional hardness value as the indent depth increases until the pressure head approaches the interface. For the small thin film thickness, see Fig.10(a) (case I), due to the strong size effect and geometrical effect, the hardness is very high, but the size effect is dominant when the indent depth is small. With increasing depth, the size effect decreases and the geometrical effect (the effect of thin film thickness and interface) increases. Until a depth equals to about 300 nm (about one fourth of thin film thickness), the geometrical effect is so large that the hardness curve turns to increase. The hardness obtains a lower limit value 5.6 GPa at the turning point. From Fig.10(b), increasing the thin film thickness by $0.6\,\mu$m, i.e., $t = 1.8\,\mu$m (case II), the geometrical effect decreases remarkably comparing with case I. For example, the hardness is about 10 GPa at $h = 100$ nm for case I, from Fig.10(a), while the corresponding hardness at the same depth is about 8 GPa for case II, from Fig.10(b). When the indent depth is small, the size effect is dominant. As the indent depth increases and the hardness decreases until the turning point at about $h = 580$ nm (about one third of the thin film thickness) is approached, from Fig.10(b). Thereafter, the geometrical effect is dominant. Considering that the thin film thickness increases and becomes very large, see Fig.10(c) (case III), the geometrical effect can be neglected. With the increase of depth, the size effect decreases. When the hardness decreases to a macro-scale hardness value, the size effect can be neglected.

In Figs.10(a), (b) and (c), the theoretical predictions of the thin film/substrate hardness from the strain gradient plasticity theory are also shown. Obviously, the characteristics of the theoretical predictions are consistent with those of the experimental results. Through plotting the theoretical predictions and the experimental results together in Figs.10(a),

(b) and (c), the dependence of the material length parameter on the thin film thickness is obtained. The corresponding values of the material length parameter are also shown in Figs.10(a), (b) and (c), respectively. Obviously, the length parameter also depends on the micro-geometrical size (thin film thickness).

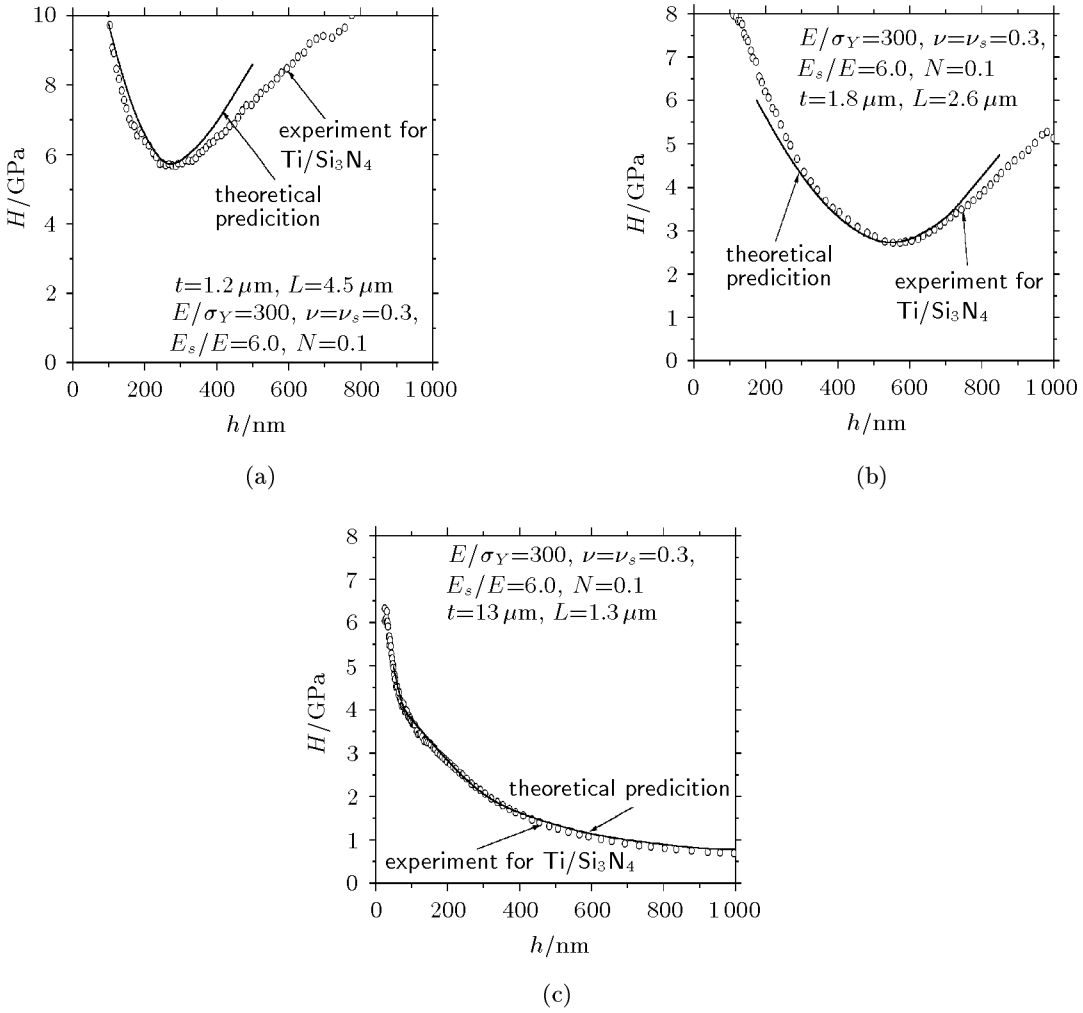

Fig.10 Experimental and numerical results of the hardness/indent depth for Ti/Si_3N_4 thin film/substrate for different thickness of thin film

7 CONCLUDING REMARKS

In the present research, the size effects and geometrical effects in the micro-indentation tests have been simulated and predicted by using the finite element implementation based on the strain gradient plasticity theory. Meanwhile, the experimental researches of the micro-indentation test for polycrystal aluminum and for the Ti/Si_3N_4 thin film/substrate structure have been carried out.

For the polycrystal material and for the thin film/substrate system, when the crystal grain size or the thin film thickness is comparable with the indent depth, the composition effects from size effect and from geometrical effect on the material hardness are considerably strong. For the hardness/depth curve, when the depth is small, the size effect is dominant. As the indent depth increases, the size effect decreases and the geometrical effect increases. Before a depth (a turning point) is reached, the geometrical effect increases, dominates and makes the hardness curve go up sharply.

The simulation results using the strain gradient plasticity theory for the size effect and the geometrical effect are consistent with experimental results. Through comparing the simulation results with experimental results, the values and the variation trends of the material length parameter included in the strain gradient plasticity theory have been predicted.

From experimental results for polycrystal Al, even though the crystal grain size is fixed, the hard-

ness/depth relation is still a scatter strip. The feature mainly comes from the status of the indenting point on the specimen surface. Certainly, it is possible that the prepared specimens always and inevitably include some faults or reinforced phases and the differences among the crystal sizes and shapes. From experimental results for Ti/Si_3N_4 thin film/substrate system using the continuum stiffness method, the composition effects of the size effect and geometrical effect are clearly displayed. The experimental results show that the material length parameter has a fixed value for a uniform material, however, when the micro-structure is considered and the length parameter increases, depending on the micro-geometrical size.

Acknowledgement A great help for preparing polycrystal Al specimen from Dr. Wu Xiaolei, is sincerely acknowledged.

REFERENCES

1 Nix WD, Gao H. Indentation size effects in crystalline materials: a law for strain gradient plasticity. *J Mech Phys Solids*, 1998, 46(3): 411∼425

2 McElhaney KW, Vlassak JJ, Nix WD. Determination of indenter tip geometry and indentation contact area for depth-sensing indentation experiments. *J Mater Res*, 1998, 13(5): 1300∼1306

3 Begley M, Hutchinson JW. The mechanics of size-dependent indentation. *J Mech Phys Solids*, 1998, 46(3): 2049∼2068

4 Shu JY, Fleck NA. The prediction of a size effect in micro-indentation. *Int J Solids Structures*, 1998, 35(13): 1363∼1383

5 Poole WJ, Ashby MF, Fleck NA. Micro-hardness tests on annealed and work-hardened copper polycrystals. *Scripta Metall Mater*, 1996, 34(6): 559∼564

6 Atkinson M. Further analysis of the size effective in indentation hardness tests of some metals. *J Mater Res*, 1995, 10(12): 2908∼2915

7 Ma Q, Clarke DR. Size dependent hardness of silver single crystals. *J Mater Res*, 1995, 10(4): 853∼863

8 Stelmashenko NA, Walls MG, Brown LM, et al. Microindentation on W and Mo priented single crystals: an STM study. *Acta Metall Mater*, 1993, 41(10): 2855∼2865

9 Wei Y, Wang X, Wu X, et al. Theoretical and experimental researches of size effect in micro-indentation test. *Science in China* (Series A), 2001, 44(1): 74∼82

10 Cheng YT, Cheng CM. Scaling relationships in conical indentation of elastic-perfectly plastic solids. *Int J Solids Structures*, 1999, 36(5): 1231∼1243

11 Fleck NA, Hutchinson JW. Strain gradient plasticity. *Advances in Applied Mechanics*, 1997, 33: 295∼361

12 Gao H, Huang Y, Nix WD, et al. Mechanism-based strain gradient plasticity——I: Theory. *J Mech Phys Solids*, 1999, 47(6): 1239∼1263

13 Aifantis EC. On the microstructural origin of certain inelastic models. *Trans ASME J Eng Mater Tech*, 1984, 106(3): 326∼330

14 Wei Y, Hutchinson JW. Steady-state crack growth and work of fracture for solids characterized by strain gradient plasticity. *J Mech Phys Solids*, 1997, 45(8): 1253∼1273

15 Timoshenko SP, Goodier JN. Theory of Elasticity. Third edition. New York: McGraw-Hill, Inc, 1970. 401

16 Shaw MC. In: McClintock FA, Argon AS, eds. Mechanical Behavior of Materials. Reading: Addison-Wesley, Mass, 1966. 443

17 Hill R. Continuum micro-mechanics of elastoplastic polycrystals. *J Mech Phys Solids*, 1965, 13(1): 89∼101

18 Xia ZC, Hutchinson JW. Crack tip fields in strain gradient plasticity. *J Mech Phys Solids*, 1996, 44: 1621∼1648

19 Chen JY, Wei Y, Huang Y, et al. The crack tip fields in strain gradient plasticity: the asymptotic and numerical analyses. *Eng Fract Mech*, 1999, 64: 625∼648

20 Wei Y. Particulate size effects in the particle-reinforced metal matrix composites. *Acta Mechanica Sinica*, 2001, 17(1): 45∼58